Journal of Energy Storage 55 (2022) 105771

Contents lists available at ScienceDirect

Journal of Energy Storage

journal homepage: www.elsevier.com/locate/est

Research papers

Operation maps in calcium looping thermochemical energy storage for concentrating solar power plants

S. Pascual, P. Lisbona *, L.M. Romeo

Mechanical Engineering Department, Escuela de Ingeniería y Arquitectura, Universidad de Zaragoza, 50018, Spain

ARTICLE INFO

Keywords:
Calcium-looping
Thermochemical energy storage
Concentrated solar power
Energy storage operation mode
Energy release operation mode
Solids separation unit

ABSTRACT

Calcium Looping (CaL) process used as thermochemical energy storage system in concentrating solar plants has been extensively investigated in the last decade and the first large-scale pilot plants are now under construction. Existing research focuses on improving global efficiencies under steady-state and single modes of operation: energy storage or energy retrieval. However, TCES systems will operate under different operation points to adapt the load of its reactors to the solar availability and the energy demand from the power cycle. A thorough analysis of the operation modes provides an extremely large number of potential situations to operate the system. In this study, operation maps which maximize thermal energy availability and energy storage efficiency are defined. Furthermore, a novel approach for the management of partially carbonated solids is examined to reduce the circulation of inert material in the system based on preliminary experimental results which allows for a partial separation of carbonated solids. Two threshold scenarios are analysed: (i) no solids separation as considered in most CaL TCES studies and (ii) ideal total solids separation. The aims of this work are to set methodological criteria to define the optimal operation map and to assess the effect of partially carbonated solids separation on the energy penalties and equipment size. The inclusion of a solid separation stage leads to a maximum increase of energy storage efficiency of 26 % and a size reduction between 53 and 74 % of those heat exchangers affected by solids streams.

1. Introduction

Half of the existing concentrated solar power (CSP) plants include thermal energy storage (TES) to maximize operating hours and electricity production [1]. Since the CSP installation cost has decreased by 70 % in the last 10 years [2], CSP plants with TES will be able to compete with conventional fossil fuel-based baseload facilities for electricity production [3]. The integration of TES in CSP plants enhances their dispatchability with variable solar radiation or during the night [4]. Literature is plenty of works about the feasible options to do this integration, some of them include current status and research trends [4], innovations [5] and specifications and pros and cons of different concentrating solar technologies [6–8] that include high (i) operating temperatures (above 1000 °C), (ii) thermodynamic efficiencies for the CSP plant and (iii) nominal power capacities [5–7]. Cost analysis has been also presented [9] demonstrating that the variability of the TES material annual costs from one year to the next is lower than fossil fuels, whose price trend is less predictable. The amount of TES stored depends on (i) the specific heat of the medium, (ii) the temperature variation and (iii) the amount of storage material option [8]. Most of the CSP plants currently under commercial operation or under construction use molten salts as a thermal storage medium [10]. Beyond molten salts, for sensible heat storage, water is also commercially used as thermal storage medium [11]. For latent heat storage, Phase Change Materials (PCMs) are used, although they show some limitations such as a low enthalpy of phase change, low thermal conductivity and instable at high temperatures [12,13]. The selection of the best TES system to each CSP technology is complex and must consider specific characteristics with regard to storage [14]. One of the preferred options is thermochemical energy storage (TCES) which makes use of the reversibility of chemical equilibrium reactions to store or to release energy through a cyclic process. TCES shows enhanced storage capacity and the minimum energy losses under seasonal storage in comparison with sensible and latent TES. Thus, TCES will be able to improve CSP conversion efficiency in the near future [15]. Moreover, TCES can also be easily integrated in CSP plants which operate above 800 °C [16,17] since it operates in the range of 450–1300 °C.

Among TCES system, the Calcium Looping process, firstly proposed

* Corresponding author.
E-mail address: pilarlm@unizar.es (P. Lisbona).

https://doi.org/10.1016/j.est.2022.105771
Received 8 July 2022; Received in revised form 31 August 2022; Accepted 26 September 2022
Available online 3 October 2022

by Baker [18], is one of the most promising. Calcination reaction of limestone, Eq. (1), is endothermic and takes place during sunlight hours at 920–950 °C [19]. Calcination products, carbon dioxide (CO_2) and calcium oxide (CaO), can be total or partially stored, diverting the remaining flowrate to the carbonator to release energy.

$$CaCO_{3\,(s)} \leftrightarrows CaO_{(s)} + CO_{2\,(g)} \quad \Delta H_R^{\circ} = +178\ kJ/mol \tag{1}$$

The energy density of $CaCO_3$ ranges between 390 and 490 kWh/t [20,21] and this value represents the main advantage of the CaL TCES technology. During night, or whenever extra thermal energy is required by the power cycle to fulfil electricity demand, the stored CO_2 and CaO may be fed into the carbonator to retrieve the stored thermal energy. The carbonation exothermic reaction, reverse Eq. (1), takes place between CO_2 and CaO at 600–850 °C [22] releasing high temperature heat. The generated $CaCO_3$ can be stored until sunlight hours when the calcination starts up again, closing the loop.

Energy storage density of CaL TCES is estimated by several authors using different definitions for comparison with other storage technologies applied to CSP plants. Sun et al. determine the energy density as the amount of stored energy per unit mass CaO (417 kWh/t after 10 cycles). In this case, the energy density is proportional to the carbonation conversion and represents the energy released in the carbonation reaction per mass CaO [23]. Di Lauro et al. define the density of energy storage for each carbonation/calcination step as the sum of (i) the chemical energy stored and (ii) the excess of sensible heat of the material respect to the discharged temperature (650 °C). The energy storage density reaches to 1419 MJ/m^3 after 10 cycles, considering a tapped bulk density of 1590 kg/m^3 for limestone. Moreno et al. established an energy storage density of 1220 MJ/m^3 after 20 cycles for limestone, considering only the chemical energy stored [24]. These values are larger than the molten salts energy storage density (800 MJ/m^3), taking into account only the sensible heat stored [25]. Other works estimate the energy storage density as the relation between (i) the energy stored as chemical, latent and sensible heat and (ii) the size of the storage tanks. The energy storage density obtained for a conventional CaL CSP system achieves 1300 MJ/m^3, which is much higher than the energy storage density of a typical molten salt with a temperature change of 275 °C (near 400 MJ/m^3) [26].

Regarding reactor design, several researchers have dealt with simulation activities for, both, carbonator [27,28] and calciner [19]. These works highlighted the importance of a proper design to evacuate the energy released during carbonation [28] and the difficulties for achieving a smooth temperature profile in the calciner [19]. New concepts based on autothermal fluidized bed reactor for calcination are investigated by Padula et al. to improve the overall TCES efficiency [29]. The advantages offered by fluidized bed technology related to gas-solid heat transfer have driven its adaptation to the new requirements of concentrated solar energy [30]. Besides, Ortiz et al. proposed an entrained flow reactor to perform the calcination under operating conditions of 765 °C and low-pressure (0.01 bar), minimizing energy losses and CaO sintering [31]. Within the potential reactors for the calcination of limestone in TCES systems (fluidized bed, entrained bed and rotary reactor), the indirectly irradiated fluidized beds seem to be the most suitable option [32]. Unfortunately, experimental results on CaL TCES pilot plants are still scarce limiting the potential validation of reactor design modelling studies [30,33]. Important issues must be addressed for the scale-up of $CaCO_3$ calcination reactors, such as the particle attrition and the high temperature resistance of the reactor wall components [32].

The CaL TCES integrated with power cycles and the optimization of the overall efficiency has been extensively investigated [34–37]. Main literature findings conclude that CO_2 power cycles provide the greatest results. The efficiencies reported for different layouts and operating conditions achieved a 40.4 % in the case of supercritical CO_2 cycles [36], and ranged between 31 and 44 % for CO_2 closed Brayton cycle [34,35,37,38]. Regarding Bryton cycles, Tesio et al. investigate the integration of two alternatives: helium and supercritical CO_2. The results show the greatest efficiency for helium cycle, whereas the supercritical CO_2 cycle is the cheapest alternative [39]. Secondly, the new improved CaL TCES designs found in literature enhance the dispatchability and minimize the cost of the CSP plants. Bravo et al. propose a hybrid solar configuration combining the CSP plant with CaL TCES with a photovoltaic (PV) plant, achieving a LCOE of 123 USD/MWh with a capacity factor of up to 73 % for the location assessed with the best solar resource [40]. Both plants produce electrical energy during the sunlight hours, partially storing energy in the CaL TCES system and covering electricity demand with part of the energy from the PV plant. The stored energy is released to cover energy demand under unavailability of solar energy [38,40]. Another way to improve the renewable share developed by Tregambi et al. is the integration of a CSP plant and CaL carbon capture technology with Power to Gas technology. The CaL process operates continuously 24 h/day, (i) storing CaO after calcination step during sunny hours and (i) feeding the CaO stored during the daytime to the carbonator when solar radiation is unavailable. The production of methane from captured CO_2 and hydrogen from water electrolysis is considered, covering the energy demand by PV plant or other renewable energy source. The overall efficiency from solar to methane production is between 20 and 22 % [41]. One of the most recently proposed configuration investigated by Ortiz et al. is based on the integration of the CaL TCES system in a combined cycle plant. The CSP plant provides solar energy to (i) the combined cycle and (i) the TCES system during the day. The energy stored in the CaL TCES system is released when solar radiation is unavailable to cover the energy demand of the power block [42]. The overall efficiency is almost 45 %, considering the solar resource of a specified location assessed [43].

In general, these studies present their results under stationary operation at nominal load with constant fractions of stored products during sunlight hours and constant operating loads of the carbonator during the night period. Nevertheless, this technology will operate under varying loads and, as a consequence, further analysis is required to describe the operational behaviour of the complete CSP plant. The amount of stored and discharged material will determine the size of heat exchangers, the transient load in the equipment and the integrations with power cycle or the use of the thermal energy as well as equipment cost and LCOE [44]. One of the novelties of this work relies in the analysis of a wide variety of the potential situations arising from the different combinations of charge/discharge fractions of the CaO, CO_2 and $CaCO_3$ storage tanks. The influence of the storage/discharge fractions on the behaviour of the plant equipment was assessed in a previous work published by the authors without considering the potential situations with simultaneous energy storage and retrieval [44]. A large number of potential operation points of the CaL-CSP system which can be operationally useful were disregarded from the previous analysis. However, the present work provides a much wider study including all the possible points and introducing a systematic methodology based on clear criteria to select and disregard the operation points under observation. Furthermore, the definition of the final operation maps in the present work maximizes the efficiency of the CaL TCES system. No research is found in literature about the optimum operational performance of CaL CSP and the different strategies to achieve high thermal energy availability or high energy storage efficiency.

Regarding energy penalties in the CaL TCES system, the circulation and storage of non-reactive solid material is one the most influential aspects on the energy efficiency of the system [45]. Low CaO activity in the carbonator leads to large amounts of inactive solid material circulating in the system [46]. A research gap also exists in the assessment of the potential reduction of inert solids circulation and storage. In this work, the effect on the energy penalty of the recirculation of partially converted CaO after carbonation reaction has been assessed.

Thus, the originality of the present work relies in (i) the establishment of optimal operation maps to guide the operation under transient

mode and (ii) the assessment of the implementation of a solids separation unit at carbonator outlet to reduce the energy demand and size of the CaL TCES system. The main objectives of the study are (i) to define adequate and methodological criteria to filter the operation points and select the feasible situations under real operation, (ii) to determine the required size and energy penalties for the optimal situations which meet technical, energy and design, equipment loads limitations and maximize significant operating parameters and (iii) to explore the effect of solids separation after carbonation reactor on the energy penalties and equipment size.

2. Systems description and operation modes

The system consists of two reactors, a calciner located inside the solar receiver and a carbonator, with intermediate storage tanks of $CaCO_3$ (ST1), CaO (ST2) and CO_2 (ST3) as illustrated in Figs. 1 and 2. A thermal input of 100 MWth to the solar calciner ($\dot{Q}_{CL}$) under nominal operation conditions is assumed considering a solar field as described in [44]. The calciner operates at atmospheric pressure and 950 °C under pure CO_2 atmosphere to ensure complete conversion [47]; thus, $CaCO_3$ is fully decomposed into CaO and CO_2. Depending on the operation mode, the CO_2 and CaO flowrates from the calciner are directed to the carbonator or diverted towards their corresponding storage tanks (ST3 and ST2).

Since CaO deactivates with the number of cycles, a stream of fresh limestone is fed in the calciner to keep a reasonable average sorption activity of the solid population. Thus, the $CaCO_3$ fed into the calciner reactor comes from both the contribution of fresh limestone and the $CaCO_3$ produced after carbonation reaction. Fresh limestone counterbalances the purged solid material (f_p) set as a percentage of the CaO molar flow formed in calcination reaction.

The carbonator operation conditions are set in 850 °C under pure CO_2 atmosphere and a pressure of 1.2 bar to improve the circulation of solids between calciner and carbonator [35]. The exothermic carbonation reaction is not complete and the average carbonation degree must be determined. The model used to determine the deactivation of the CaO particles is tuned adjusting the kinetic model described by Grasa et al. [48] obtained for 650 °C and an approximately CO_2 concentration between 10 and 15%vol. The amount of carbonated CaO and the energy released ($\dot{Q}_{CR}$) will depend on the average sorption activity of the population of particles circulating in the system [49]. Therefore, a mixture of $CaCO_3$ and CaO consisting of partially carbonated lime particles which present a range of densities between 2762 and 2930 kg/m^3 is found at carbonator outlet [50]. This experimentally measure density difference for the cycled particles points out the existing potential for partial separation of these particles through fluidization processes. The CaO to CO_2 molar ratio introduced in the carbonator (R) and the average sorbent activity define the carbon capture efficiency in the carbonator reactor.

CO_2 is stored at 35 °C and 75 bar. The CO_2 compression-train includes four interleaved compression and cooling stages. The first three cooling stages reduce the temperature to 50 °C and the last stage down to the storage temperature, 35 °C. A pressure ratio of 3 is considered in each compression stage which limits the electricity consumption and makes use of the heat released in the cooling stages. The CO_2 discharged from the tank ST3 must reduce its pressure (75 bar) to the carbonator working pressure (1.2 bar) through an expansion valve (EV). Besides, the temperature of the discharged CO_2 is increased up to ambient temperature (HEAMB) before being introduced to the ER-CO2 heat exchanger. Depending on the operation mode, the CO_2 from the storage tank ST3 is mixed with CO_2 from calciner before being introduced into carbonator at 850 °C. Regarding solids storage conditions, lime and limestone storage temperature may range from ambient to 200–700 °C [34]. Storage temperature and pressure of solids are set at 200 °C and 1 bar. Both scenarios have been simulated with Engineering Equation Solver (EES) software [51], using internal data library for CO_2 properties and external data sources for solids substances: lime [52] and limestone [53].

Lastly, a network of heat exchangers (HE) will supply or remove thermal energy according to the operation mode of the CaL TCES system. Heat exchangers designated as EE, Figs. 1 and 2, are able to provide energy under any mode of operation with heat losses of a 2 %. However, the heat exchanger designated as ER-CaCO3 always requires thermal energy input while the rest of ER heat exchangers provide or demand energy depending on the operation mode. The heat exchange network will be designed to cover the thermal energy required by (i) heat exchangers named ER and (ii) an associated power block to produce electricity. Only the heating and cooling needs have been calculated. The thermal integration is beyond the scope of the present study and will be assessed in future works.

In this study, the CaL TCES system has been analysed under two threshold scenarios which consider (SC1) no separation of solids of the solid stream leaving the carbonator, Fig. 1, and (SC2) an ideal and total separation of the solid CaO-$CaCO_3$ mixture generated in the carbonator, Fig. 2. Carbonation occurs on the surface of the particle producing a mixture of partially carbonated particles, thus, complete separation of CaO and $CaCO_3$ will never effectively happen and SC2 represents an unreal situation. However, it is used in the study as a threshold situation to easily estimate a minimum energy consumption and size of the equipment. The operating conditions of the main equipment in the CaL

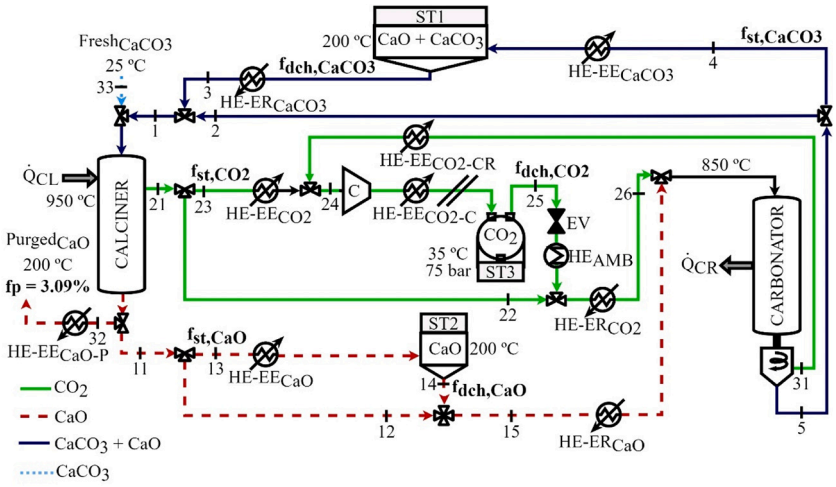

Fig. 1. CaL TCES system for a 100 MWth CSP plant w/o solid separation (SC1).

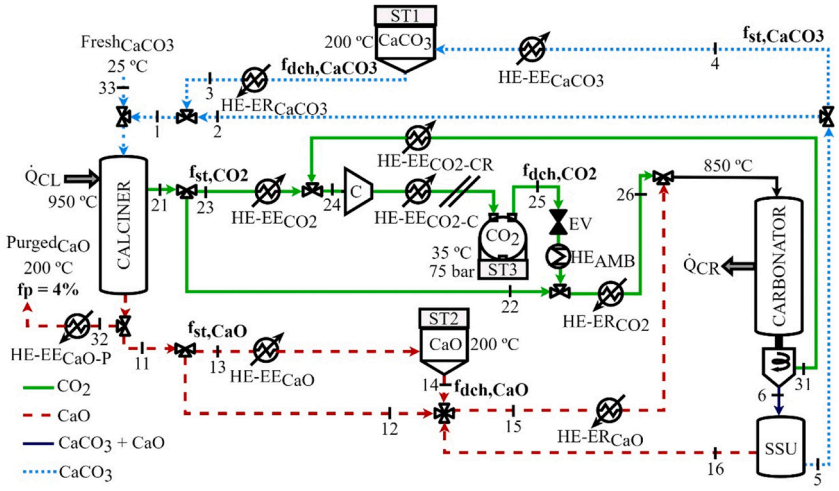

Fig. 2. CaL TCES system under total solids separation (SSU) scenario (SC2).

TCES system (calciner, carbonator, storage tanks, heat exchangers and compression-cooling train) are the same under both scenarios. The molar ratio between CaO and CO_2 (R) is set as 4.26 in both scenarios [27], leading to a f_p of 3.09 % and 4 % for SC1 and SC2, respectively. Besides, an average sorption activity of 20.4 % and 22.6 % is estimated for the sorbent under SC1 and SC2, respectively, considering a residual conversion of 7.5 % and a deactivation constant of 0.52 for the selected limestone, X_N, and a conservative age distribution of solid population as provided by Pascual et al. [44]. The different mass balances in the CaL TCES systems and the relevant performance parameters are described under both threshold scenarios.

2.1. CaL TCES w/o solid separation unit (Scenario 1 - SC1)

The first scenario does not consider solid separation at the outlet of the carbonator and is illustrated in Fig. 1. Under SC1, the input of solid particles to the calciner which must be heated up to 950 °C consists of a mixture of around 80 % lime and 20 % limestone and comes from the carbonator at 850 °C and the storage tank ST1 at 200 °C. The inlet stream of solids directed to the carbonator results from the mixture of the CaO stream discharged from storage tank ST2 (200 °C) and the direct CaO flowrate from calciner (950 °C).

Only a share of the solar input is used to calcine the limestone introduced in the calciner while a large amount of heat is invested in heating the CaO/$CaCO_3$ solid mixture up to 950 °C. For this reason, the lower amount of CaO in the inlet solid mixture, the higher amount of calcined limestone and, therefore, the higher chemical energy stored in the solid stream leaving the calciner. Besides, the amount of solid particles circulating between reactors is significantly reduced, so the involved heat exchangers and storage tanks decrease their size.

The specific thermal energy required in the calciner is 2169.5 kJ/kg $CaCO_3$ for a system without solids separation unit (SC1) and 1906.6 kJ/kg $CaCO_3$ for a system with ideal and complete solids separation (SC2). This significant reduction of heat demand is related to the lower preheating needs for the solids stream introduced in the calciner.

2.2. CaL TCES with solid separation unit (Scenario 2 - SC2)

The second scenario under study considers the ideal situation of total solid separation at carbonator outlet (SC2) as shown in Fig. 2. This unreal solids separation assumes the total separation of the solid mixture into two pure streams of $CaCO_3$ and CaO. In particular, the solid separation unit (SSU) receives the CaO/$CaCO_3$ mixture from the carbonator and separates (i) the unreacted CaO which is recirculated into the carbonator and (ii) the limestone stream sent back to the calciner or to the $CaCO_3$ storage tank (ST1). This scenario will be useful to analyse the threshold values of equipment size and energy consumptions under the most advantageous case.

Under this second theoretical scenario, the calciner is only fed with $CaCO_3$ in the solid inlet stream. Thus, the solar energy input is fully used to heat the limestone up to 950 °C and calcine the solid material. No solar energy is wasted in the heating of calcined material, CaO. For this reason, the amount of calcined limestone is increased for the same calciner power while the circulation of solids between reactors is reduced. The unreacted CaO after carbonation is separated and recirculated into the carbonator itself.

The greatest influence of the solid separation unit affects the equipment shown in Fig. 2: (i) the heat exchangers with solids streams involved (EE-CaO, ER-CaO, EE-CaCO3 and ER-CaCO3) and (ii) mainly CaO and $CaCO_3$ storage tanks (ST2 and ST1).

2.3. Operation modes

Depending on the availability of solar energy and/or the demand of thermal energy required from the CaL TCES, the management of the gas and solids streams to and from the storage tanks will follow a different operation mode. Under both scenarios (SC1 and SC2), three operation modes are analysed: (i) energy storage operation mode (ESOM), (ii) direct operation mode (DOM) and (iii) energy retrieval operation mode (EROM).

2.3.1. Storage and discharge fractions

The operation under nominal power in the calciner, 100 MWth, provides the maximum available energy to be stored. Moreover, the maximum retrieved power will be achieved under nominal operation in the carbonator determined considering the direct operation of the carbonation-calcination cycle. The chemical energy content of the solid stream generated in the calciner under nominal conditions amounts to 69 MWth under SC1 and 88 MWth under SC2. This energy will be totally recovered in the carbonator under direct operation and represents the maximum released power and the nominal power in the carbonator. The maximum mass flows of gas and solids obtained when reactors operate at nominal power are presented in Table 1.

The maximum CO_2 and CaO flowrates ($\dot{m}_{st,max,CO2}$, $\dot{m}_{st,max,CaO}$) diverted to or discharged from the storage tanks ST3 and ST2 corresponds to the maximum CO_2 and CaO flowrates leaving the calciner when it operates at nominal power. The flowrates of CO_2 and CaO received in the storage tanks ST3 and ST2 ($\dot{m}_{st,CaO}$, $\dot{m}_{st,CO2}$) will correspond to a fraction of these maximum CO_2 and CaO streams, Eq. (2). The CO_2 and CaO leaving the storage tanks ST3 and ST2 ($\dot{m}_{dch,CaO}$, $\dot{m}_{dch,CO2}$)

Table 1
Mass flow of gas and solids under calciner and carbonator nominal powers.

Nominal power and mass flow description			No separation (SC1)	Total separation (SC2)
$P_{nom,CL}$	(MW)	Nominal power calciner	100	100
$P_{nom,CR}$	(MW)	Nominal power carbonator	69	88
$\dot{m}_{st,max,CO2}$	(kg/s)	Maximum mass flow CO_2 from CL	21.16	24.35
$\dot{m}_{st,max,CaO}$	(kg/s)	Maximum mass flow CaO from CL	114.77	29.83
$\dot{m}_{st,max,CaCO3}$	(kg/s)	Maximum mass flow CaO/$CaCO_3$ from CR	133.15	53.24[a]

[a] Only $CaCO_3$ from SSU.

are also defined as a fraction of the maximum CO_2 and CaO streams at calciner outlet, Eq. (3).

$$f_{st,CaO} = \frac{\dot{m}_{st,CaO}}{\dot{m}_{st,max,CaO}} = \frac{\dot{m}_{13}}{\dot{m}_{st,max,CaO}} \quad (2)$$

$$f_{dch,CaO} = \frac{\dot{m}_{dch,CaO}}{\dot{m}_{st,max,CaO}} = \frac{\dot{m}_{14}}{\dot{m}_{st,max,CaO}} \quad (3)$$

The maximum CaO/$CaCO_3$ flowrate ($\dot{m}_{st,max,CaCO3}$) diverted to or discharged from the storage tank ST1 corresponds to the maximum CaO/$CaCO_3$ flowrate leaving the carbonator when it operates at nominal power (69 MWth and 88 MWth for SC1 and SC2, respectively). The CaO/$CaCO_3$ stream received in the storage tank ST1 ($\dot{m}_{st,CaCO3}$) will correspond to a fraction of this maximum CaO/$CaCO_3$ flowrate, Eq. (4). The CaO and $CaCO_3$ leaving the storage tank ST1 ($\dot{m}_{dch,CaCO3}$) are defined as a fraction of the maximum mixture of CaO and $CaCO_3$ stream at carbonator outlet, Eq. (5).

$$f_{st,CaCO3} = \frac{\dot{m}_{st,CaCO3}}{\dot{m}_{st,max,CaCO3}} = \frac{\dot{m}_{4}}{\dot{m}_{st,max,CaCO3}} \quad (4)$$

$$f_{dch,CaCO3} = \frac{\dot{m}_{dch,CaCO3}}{\dot{m}_{st,max,CaCO3}} = \frac{\dot{m}_{3}}{\dot{m}_{st,max,CaCO3}} \quad (5)$$

2.3.2. Operation modes

The operating points for a given pair of calciner/carbonator loads are defined through the storage/discharge fractions. The maximum storage and discharge fraction as defined above are theoretical thresholds which, in this study, have been assumed as 1.

When the system is operated as Energy Storage Operation Mode (ESOM), the input of solar power is assumed to be equal or lower than the calciner nominal power, while the power released in the carbonator will be always below its nominal power for both SC1 and SC2. During this operation mode, the resulting CaO and CO_2 streams from calciner are partially or totally stored and the CaO and CO_2 storage fractions ($f_{st,CaO}$, $f_{st,CO2}$) are always higher than the discharge fractions ($f_{dch,CaO}$, $f_{dch,CO2}$). It is considered that no solids from the carbonator are diverted to storage ($f_{st,CaCO3} = 0$) under ESOM. Thus, the feasible operating points for each pair of carbonator/calciner loads are defined by a given discharge fraction of $CaCO_3$ ($f_{dch,CaCO3}$) and a range of storage fractions of CaO and CO_2. The minimum and maximum values of these fractions are presented in Table 2.

Under the Energy Retrieval Operation Mode (EROM), the solar power input in the calciner is considered to be below its nominal power. The thermal power released in the carbonator can be equal to or lower than its nominal power for each studied scenario (SC1 and SC2). The $CaCO_3$ storage fraction ($f_{st,CaCO3}$) is always higher than the $CaCO_3$ discharge fraction ($f_{dch,CaCO3}$) at all possible energy release operating points for each pair of calciner/carbonator loads. It is considered that no gas or solids from the calciner are diverted to storage ($f_{st,CaO} = 0$) under EROM. The technically operating points for each pair of reactor loads are defined by a given discharge fraction of CaO ($f_{dch,CaO}$) and a range of storage fractions of $CaCO_3$. The minimum and maximum values of these fractions are also shown in Table 2.

The third operation mode, Direct Operation Mode (DOM), presents a direct circulation between reactors without net storage or discharge of CaO $CaCO_3$ and CO_2. The calciner and carbonator are operated at the same load with respect to their respective nominal powers under DOM. This operation mode is not useful for TCES but for its implementation for carbon capture processes.

Table 2
Definition of operation modes of the TCES system.

Operation parameters	Energy operation modes	
	ESOM	EROM
$\dot{Q}_{CL}$ (MW)	$\leq P_{nomCL}$	$< P_{nomCL}$
$\dot{Q}_{CR}$ (MW)	$< P_{nomCR}$	$\leq P_{nomCR}$
$Load_{CL}$ (−)	≤ 1	0 to $< L_{CR}$
$Load_{CR}$ (−)	0 to $< L_{CL}$	≤ 1
$f_{st,CaO}$ (−)	$f_{dch,CaCO3}$ to L_{CL}	0
$f_{dch,CaO}$ (−)	0 to L_{CR}	(L_{CR}-L_{CL})
$f_{st,CaCO3}$ (−)	0	$f_{dch,CaO}$ to L_{CR}
$f_{dch,CaCO3}$ (−)	(L_{CL}-L_{CR})	0 to L_{CL}

Table 2 summarizes the information for the different operating variables of the operating modes of the system described above (ESOM and EROM).

Thus, an operation point is completely defined by a pair of reactor loads (L_{CL}, L_{CR}) and the storage fraction of CaO/CO_2 ($f_{st,CaO}$) under ESOM and the storage fraction of $CaCO_3$ ($f_{st,CaCO3}$) under EROM. The rest of discharge and storage fractions are dependant of these parameters.

3. Criteria for operation point selection

The operation points included in the operation map of the CaL TCES system are narrowed down according to following aspects: the heat exchange equipment size, the carbonator load and thermal energy availability and the storage energy efficiency.

3.1. Design and technical criteria

Several situations are detected to be not technically feasible or energetically or economically disadvantageous. Thus, several criteria are established to narrow down the amount of studied operation points:

C.1. Under ESOM, it is assumed that no limestone is stored in ST1 ($f_{st,CaCO3} = 0$) while, under EROM, no lime is diverted to the storage tank ST2 ($f_{st,CaO} = 0$).
C.2. The operating points corresponding to the direct operation modes are discarded given the energy penalty imposed by the operation of the CaL system without producing a net thermal energy storage or retrieval.
C.3. Only those operating points in which ER-HE heat exchangers demand energy are considered technically suitable for the design of the facility.
C.4. A minimum partial load is required for the operation of the carbonator and the heat exchangers involved in the system to ensure the continuous operation of the CSP power block. The minimum operation load is set at 50 % for system equipment with nominal released power >15 MW (carbonator, EE-CO2, EE-CaO and EE-CaCO3).

C.5. A maximum energy demand is established for the ER-CaCO3 heat exchanger to limit its energy consumption and size. This threshold value is set as the 50 % of the maximum heat requirement in ER-CaCO3 obtained among the operation points analysed after C.3.

The performance of the system is only assessed for those operation points selected after the application of these five criteria. The selection of the most interesting points for each pair of loads (L_{CR}, L_{CL}) to define the operation map will be based on the evaluation of the thermal energy availability (η_{av}) and the storage energy efficiency (η_{st}).

3.2. Definition of energy availability, storage efficiency and specific storage consumption

Three parameters are defined to characterize the performance of the system depending on the mode of operation: the thermal energy availability, the storage efficiency and the specific storage consumption. The thermal energy availability ratio compares the available thermal energy of the system to the invested energy input. The storage efficiency compares the amount of stored energy and the net energy consumed during the storage process. The specific storage consumption presents the total amount of energy (thermal and electrical) required to store a mass unit of lime.

Under EROM, the thermal energy availability of the system is defined by Eq. (6). The available heat includes the thermal power from the carbonator and EE heat exchangers. The energy invested in this process includes (i) the heat of calcination demanded in the calciner, $\dot{Q}_{CL}$, (ii) the energy consumption related to the storage step of the lime discharged from the tank ST2, (iii) the thermal power demand in the heat exchangers named ER.

$$\eta_{av(EROM)} = \frac{\dot{Q}_{CR} + \sum \dot{Q}_{HE\ EE}}{\dot{Q}_{CL} + \sum \dot{Q}_{HE\ ER} + SSC \bullet \dot{m}_{CaO,dch}} \tag{6}$$

The total energy input to the system under ESOM only includes the required heat in the calciner, $\dot{Q}_{CL}$, and the heat demanded to preheat the gas and solid mass flowrates through the heat exchangers named ER. This thermal energy availability is defined by Eq. (7).

$$\eta_{av(ESOM)} = \frac{\dot{Q}_{CR} + \sum \dot{Q}_{HE\ EE}}{\dot{Q}_{CL} + \sum \dot{Q}_{HE\ ER}} \tag{7}$$

The storage efficiency may be calculated through Eq. (8). The stored energy accounts for the sensible heat of the stored material and the chemical energy stored in the lime which will be latter carbonated. The energy invested in the process includes the calcination heat required to produce the lime sent to ST2 ($\dot{Q}_{CL,st}$), the energy to preheat of the amount of limestone discharged from the storage tank ST1 which is later stored as lime in ST2 ($\dot{Q}_{HE\ ER\ CaCO3,st}$) and the electric power consumed in the compression of the stored carbon dioxide ($\dot{W}_{compressor}$). This parameter provides an estimation of the share of stored energy in comparison to the energy invested during the storage process.

$$\eta_{st} = \frac{\dot{Q}_{st,CaO}}{\dot{Q}_{CL,st} + \dot{Q}_{HE\ ER\ CaCO3,st} + \dot{W}_{compressor}} = \frac{SH_{CO2+CaO,st} + \Delta H_R^0 \bullet \dot{n}_{CaCO3,CR}}{\dot{Q}_{CL,st} + \dot{Q}_{HE\ ER\ CaCO3,st} + \dot{W}_{compressor}} \tag{8}$$

The specific storage consumption (*SSC*), Eq. (9), indicates the energetic feasibility of the storage process under specific operation points. It must be kept in mind the qualitative interest of the parameter but its limitation as quantitative measure given the mix of energy types in its definition.

$$SSC = \frac{\dot{Q}_{CL,st} + \dot{Q}_{HE\ ER\ CaCO3,st} + \dot{W}_{compressor}}{\dot{m}_{CaO,st}} \tag{9}$$

4. Results and discussion

The operation points to be analysed are narrowed down based on initial assumptions and technical criteria. Once the number of cases are reduced, the energy availability ratio and storage efficiency are calculated to assess the most advantageous operation point for a given pair of calciner/carbonator loads.

4.1. Matrix of potential operational points

Each pair of reactors loads determines the net energy to be stored and/or discharged but a large number of operating points with different storage and discharge fractions may lead to the same net energy storage or release situation. However, the energy demand or availability in the different components of the system (heat exchangers, compressor) will vary depending on the values of the storage and discharge fractions. In this section, possible operating points are selected using those criteria previously defined.

Table 3 summarizes the range size of the heat exchangers and compressor-cooling train of the possible operation points applying criteria (C.1), (C.2) and (C.3). The sign (−) means heat power release or electric power demand whereas the sign (+) means the equipment requires heat.

The minimum load in the carbonator and the heat exchangers EE-CO2, EE-CaO and EE-CaCO3 is set at 50 % by Criterion 4 (C.4). The nominal power of each equipment corresponds to the values presented maximum in the column [Max] of Table 3 under both scenarios. The carbonator operates above 50 % of its nominal power under both operation modes (ESOM and EROM).

Regarding the heat exchangers, the minimum partial load for EE-CO2 and EE-CaO under the ESOM will be 50 % of their nominal power while EE-CaCO3 will be disconnected. Under EROM, EE-CaCO3 heat exchanger will operate above 50 % of its nominal power while EE-CO2 and EE-CaO are disconnected. On the other hand, the ER-CaO and ER-CO2 heat exchangers are dependent on the load of the carbonator and, therefore, of the CaO and CO_2 inlet flowrate in the carbonator, respectively. While the ER-CaCO3 heat exchanger will be designed to always work below a 50 % of the maximum energy requirement, (C.5). Fig. 3 illustrates the number of operation points discretizing the storage and discharge fractions from 0 to 1 in ten steps after also applying from (C.1) to (C.5).

The operating points, considering a minimum partial load of 50 % in the mentioned equipment and limiting the size of ER-CaCO3, amount to 69 points within ESOM and 114 points under EROM. The thermal energy availability and the energy storage efficiency will be calculated for all these operation points to provide information about the most favourable operation map when the following objectives are pursued within the system: (i) the maximization of the thermal energy availability (EROM) or (ii) the maximization of the energy storage efficiency (ESOM).

4.2. Thermal energy availability – Energy Retrieval Operation Mode

First, the operation map which maximizes thermal energy availability is determined. This parameter becomes especially relevant when the system is operated to recover the stored energy, EROM. The thermal energy availability was calculated for all the operating points shown in Fig. 3 and, then, those which led to the highest values were selected to create this operation map. For each pair of carbonator/calciner loads, the thermal energy availability is computed by Eq. (6) when energy retrieval takes place (EROM). The maximum thermal energy availability and the power discharged from storage tanks under both solid management scenarios (SC1 and SC2) are illustrated in Fig. 4.

Under both scenarios, the maximum thermal energy availability diminishes for lower calciner and higher carbonator loads. The maximum thermal energy availability range between 0.56 and 0.86 for SC1 and

Table 3
Ranges of plant equipment size after applying C.1, C.2 and C.3.

Energy flow description				SC1 - w/o SS		SC2 - 100%SS	
				Min	Max	Min	Max
Heat exchanger		T_{in}[a] (°C)	T_{out} (°C)	$\dot{Q}$ (MW)			
CO_2	EE-CO_2	950	50	−21.14	0.00	−24.33	0.00
	∑EE-CO2-Ci	145–150[b]	50–35[b]	−10.75	−0.13	−11.44	−0.04
	EE-CO_2-CR	850	50	−2.46	−0.13	−0.82	−0.08
	ER-CO_2	950/15	850	19.52	0.00	22.46	0.00
CaO	EE-CaO	950	200	−78.88	0.00	−20.50	0.00
	EE-CaO-P	950	200	−2.44	0.00	−0.82	0.00
	ER-CaO	950/200/850[c]	850	69.32	0.00	18.01	0.00
$CaCO_3$	EE-$CaCO_3$	850	200	−85.86	0.00	−40.51	0.00
	ER-$CaCO_3$	200	850	87.61	0.00	41.34	0.00

Compressor train		T_{in}[a] (°C)	T_{out} (°C)	$\dot{W}$ (MW)			
CO_2 comp	∑C_i (up to 75 bar)	50	145–150[b]	−7.89	−0.09	−8.41	−0.03

[a] Several streams at different temperatures can be fed into a heat exchanger (T_1/T_2).
[b] The temperature of this stream may vary within a range (T_1-T_2).
[c] The stream at 850 °C is only fed to ER-CaO under SC2 since it corresponds to the recirculation from SSU to CR.

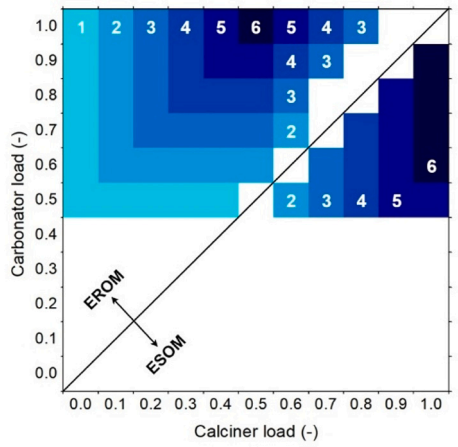

Fig. 3. Operation points distribution respect to calciner and carbonator loads under C.1., C.2, C.3, C.4 and C.5.

0.67 and 0.91 for SC2. The power retrieved from storage under EROM for both scenarios is also illustrated in Fig. 4. The lower power discharge, the higher the thermal energy availability for SC2 compared to SC1. The circulation of solids through the HE-ER-CaO is greater in SC1 than in SC2, so the energy required increases.

The operation map which maximizes the thermal energy availability is presented in the following, Fig. 5. Under EROM, the significant parameters which define an operation point are storage and discharge fractions of $CaCO_3$ ($f_{st,CaCO3}$, $f_{dch,CaCO3}$). As presented in Fig. 5, different operation maps are obtained for each scenario (SC1 and SC2) to maximize the thermal availability. The maximum thermal availability is achieved under more favourable conditions when solid separation is included (SC2). Under SC2, a lower amount of solids is sent to the storage tank of limestone (ST1) leading to smaller sizes of this equipment and a lower amount of solids is discharged from the tank implying a more limited energy penalty related to the preheating of this stream.

The range size of the equipment involved in the system for both scenarios is presented in Table 4. The negative sign (−) of the thermal power for a heat exchanger indicates an energy release, while a positive value (+) means that a specific heat exchanger requires an energy input.

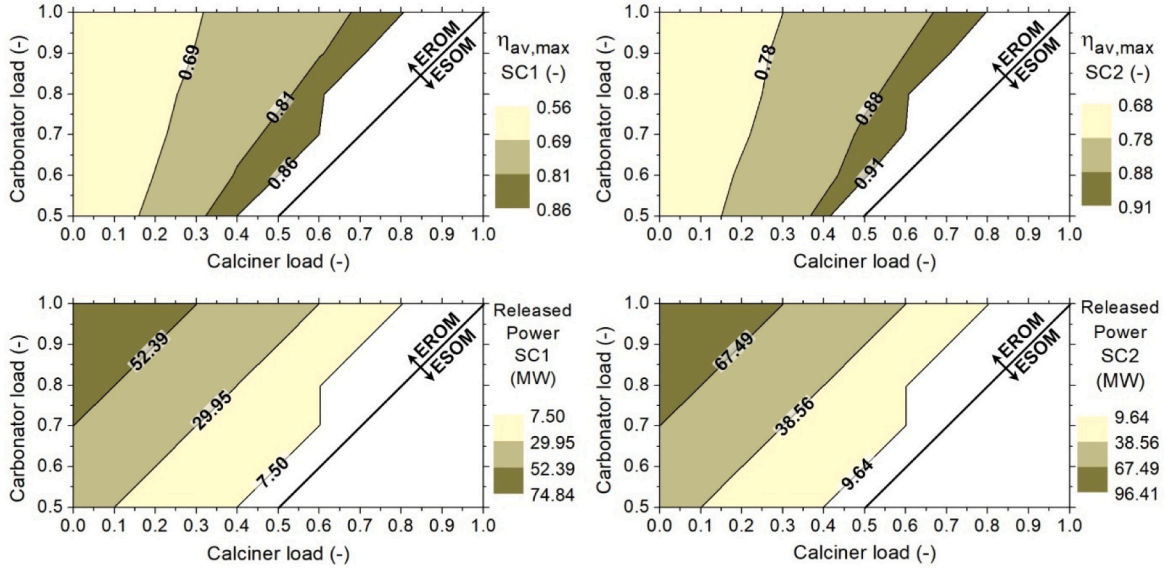

Fig. 4. Maximum thermal energy availability and released power under SC1 and SC2.

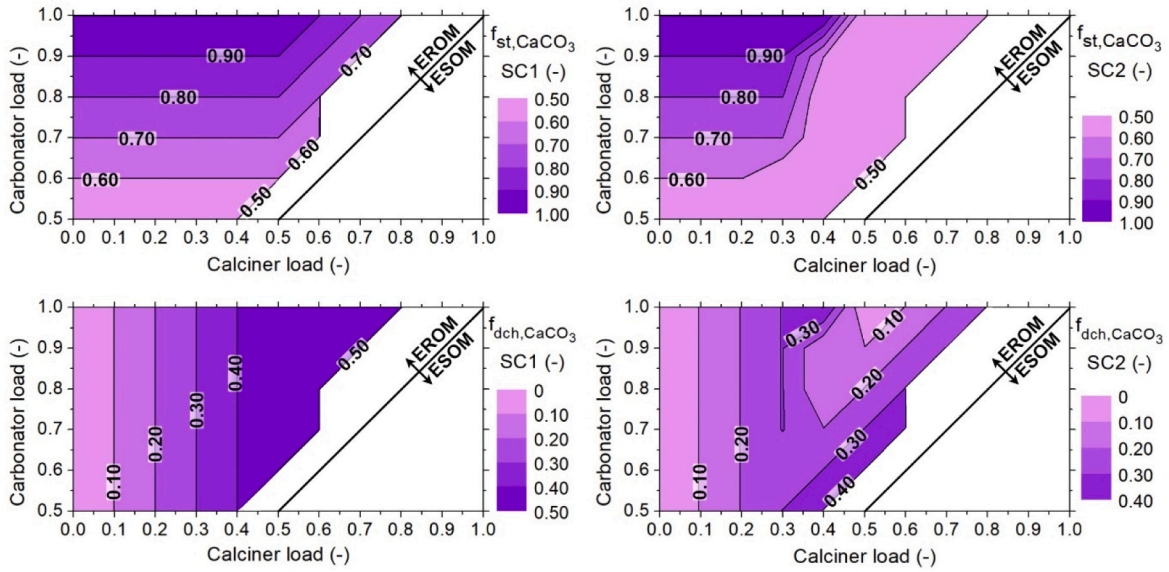

Fig. 5. Operation map under EROM (left: SC1 and right: SC2).

Table 4
Range size of plant equipment under maximization of available energy efficiency.

Energy flow description				SC1 - w/o SS		SC2 - 100%SS	
				Min	Max	Min	Max
Heat exchanger		T_{in}[a] (°C)	T_{out} (°C)	$\dot{Q}$ (MW)			
CO_2	EE-CO_2	950	50	−21.14	0.00	−24.33	0.00
	∑EE-CO2-Ci	145–150[b]	50–35[b]	−10.75	−0.63	−11.44	−0.21
	EE-CO_2-CR	850	50	−2.46	−1.22	−0.82	−0.41
	ER-CO_2	950/15	850	19.52	0.33	22.46	0.38
CaO	EE-CaO	950	200	−78.88	0.00	−20.50	0.00
	EE-CaO-P	950	200	−2.44	0.00	−0.82	0.00
	ER-CaO	950/200/850[c]	850	69.32	0.22	18.01	0.06
$CaCO_3$	EE-$CaCO_3$	850	200	−85.86	0.00	−40.51	0.00
	ER-$CaCO_3$	200	850	43.81	0.00	20.67	0.00

Compressor train		T_{in}[a] (°C)	T_{out} (°C)	$\dot{W}$ (MW)			
CO_2 comp	∑C_i (up to 75 bar)	50	145–150[b]	−7.89	−0.46	−8.41	−0.16

[a] Several streams at different temperatures can be fed into a heat exchanger (T_1/T_2).
[b] The temperature of this stream may vary within a range (T_1-T_2).
[c] The stream at 850 °C is only fed to ER-CaO under SC2 since it corresponds to the recirculation from SSU to CR.

The negative sign (−) of the electric power for the compressor train means an energy demand.

Only the energy consumed by the heat exchanger ER-CaCO3 is reduced by 50 % under both scenarios with respect to the maximum reference power that appears in Table 3, which is obtained after applying the criteria (C.1), (C.2) and (C.3). However, the energy is more efficiently recovered under SC2 than SC1.

4.3. Energy storage efficiency – Energy Storage Operation Mode

Under energy storage operation modes (ESOM), the most relevant parameter to assess the performance of the system is the stored energy efficiency. Thus, an operation map which maximizes the energy storage efficiency is also determined. The energy storage efficiency has been defined through Eq. (8) for the operating points under energy storage mode shown in Fig. 3 and the maximum values of storage efficiency for each pair of calciner/carbonator loads for both scenarios are illustrated in Fig. 6. The amount of stored energy is always the same for a given pair of calciner/carbonator loads, independently of the storage and discharge fractions.

The maximum energy storage efficiency range between 0.48 and 0.62 for SC1 and 0.64 and 0.76 for SC2. The greater amount of stored energy, the greater energy consumed. However, the energy storage efficiency for SC2 is clearly above the values obtained under SC1. The energy consumed in preheating the unconverted CaO before the calcination reaction disappear under SC2.

The specific storage consumption for each pair of calciner/carbonator loads is represented in Fig. 7. The values of SSC range between 5.93 and 6.60 MJ/kg for SC1 and 4.24 and 4.98 MJ/kg for SC2. The CO_2 flow through the compression-cooling train decreases due to the storage and discharge fractions of CaO and CO_2 ($f_{st,CaO}$, $f_{dch,CaO}$) are the minimum possible within the evaluated points. Thus, the electric energy consumption drops.

The greater energy storage efficiency (see Fig. 6), the less specific storage consumption. However, the SSC range for SC1 is above the values obtained in SC2. The maximum possible CaO flow rate to be stored under both scenarios corresponds to the CaO produced after $CaCO_3$ calcination. Under SC2 the $CaCO_3$ flow rate to be calcined is

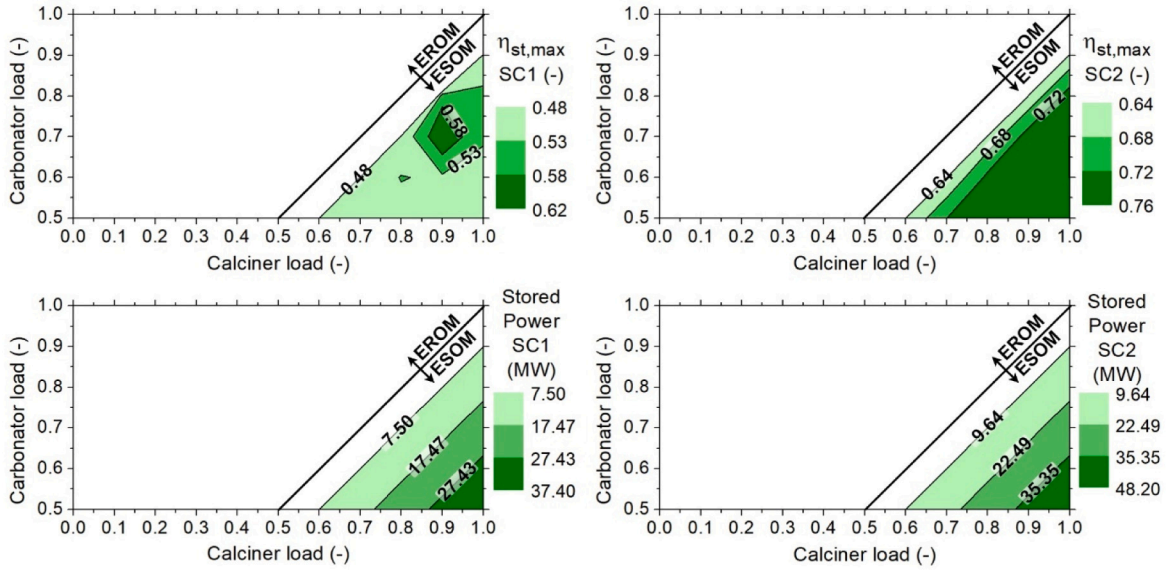

Fig. 6. Maximum energy storage efficiency and stored power under SC1 and SC2.

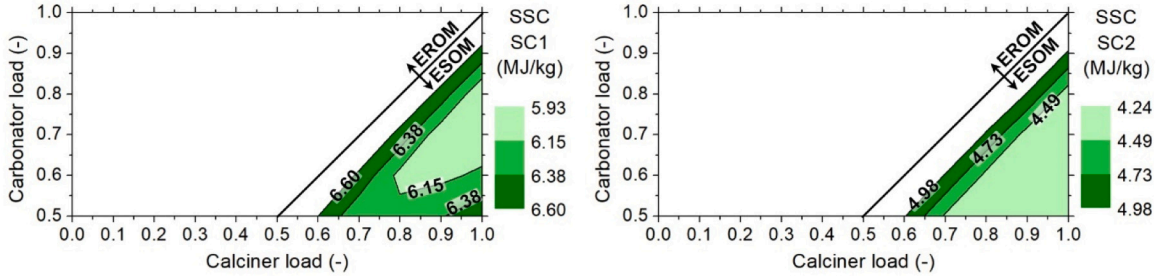

Fig. 7. Minimum specific storage consumption under SC1 and SC2.

approximately 20 % greater than in SC1 because 'inert' solids do not circulate through the system (all the material introduced in calciner is limestone). Therefore, energy requirements are higher in SC1 than in SC2 due to unconverted CaO from carbonator is stored and discharged from storage tanks ST1 and ST2.

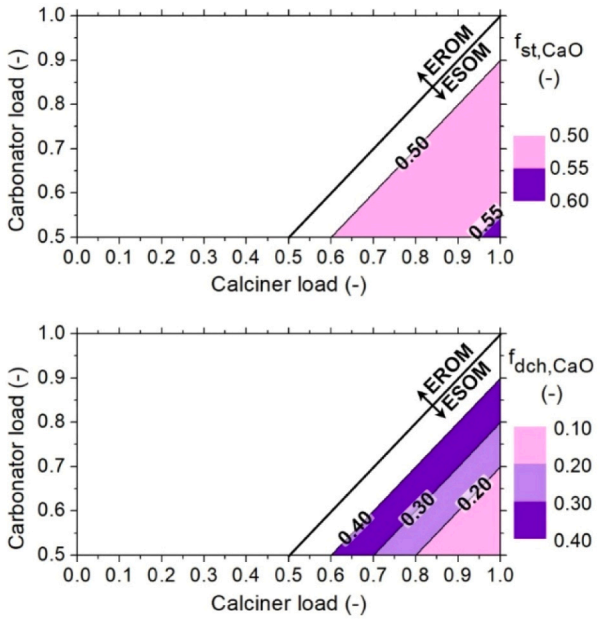

Fig. 8. Operation map under ESOM (SC1 and SC2).

The operation map which maximizes the energy storage efficiency has only sense under ESOM and it is shown in Fig. 8. This operation map defined by the storage and discharge fractions of CaO and CO_2 ($f_{st,CaO}$, $f_{dch,CaO}$) is equivalent for both solid management scenarios (SC1 and SC2).

The values of thermal energy availability of the operation map defined for each pair of calciner/carbonator loads are represented in Fig. 9. The thermal energy availability ranges between 0.71 and 0.90 for SC1 and 0.64 and 0.93 for SC2.

The range size of the equipment involved in the system for both scenarios is presented in Table 5. The negative sign (−) of the thermal power for a heat exchanger indicates an energy release, while a positive value (+) means that a specific heat exchanger requires an energy input. The negative sign (−) of the electric power for the compressor train means an energy demand.

The ER-CaCO3 heat exchanger keeps the size reduction by 50 % under both scenarios with respect to the maximum reference power that appears in Table 3, which is obtained after applying the minimum partial load criterion. Besides, under both scenarios the maximum size of the EE-CaO and EE-CO2 heat exchangers and the compression-cooling train is reduced by 40 % respect to the maximum reference power represented in Table 3. The maximization of the energy storage efficiency implies a lower energy consumption. For a pair of calciner/carbonator loads, the maximum energy storage efficiency is reached when (i) the electricity consumed by compressor train is small and (ii) the CaO and CO_2 storage fraction is the minimum possible to achieve the energy

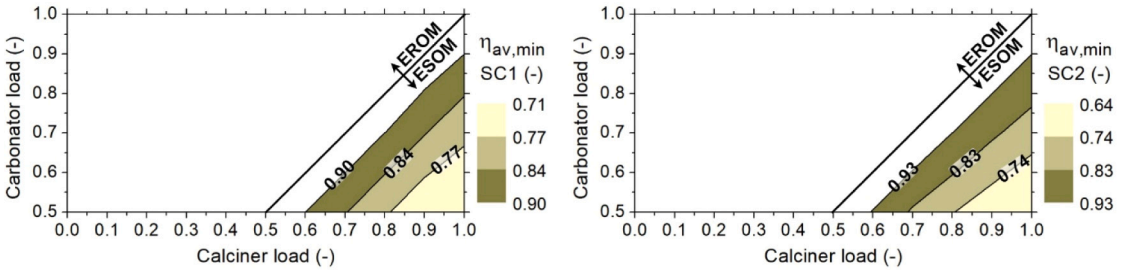

Fig. 9. Thermal energy availability and released power (SC1 and SC2).

Table 5
Range size of plant equipment under maximization of energy storage efficiency.

Energy flow description				SC1 - w/o SS		SC2 - 100%SS	
				Min	Max	Min	Max
Heat exchanger		T_{in}[a] (°C)	T_{out} (°C)	$\dot{Q}$ (MW)			
CO_2	EE-CO_2	950	50	−12.69	0.00	−14.60	0.00
	∑EE-CO2-Ci	145–150[b]	50–35[b]	−6.40	−0.63	−6.85	−0.21
	EE-CO_2-CR	850	50	−2.46	−1.22	−0.82	−0.41
	ER-CO_2	950/15	850	19.52	0.33	22.46	0.38
CaO	EE-CaO	950	200	−47.33	0.00	−12.30	0.00
	EE-CaO-P	950	200	−2.44	0.00	−0.82	0.00
	ER-CaO	950/200/850[c]	850	69.32	0.22	18.01	0.06
$CaCO_3$	EE-$CaCO_3$	850	200	−85.86	0.00	−40.51	0.00
	ER-$CaCO_3$	200	850	43.81	0.00	20.67	0.00

Compressor train		T_{in}[a] (°C)	T_{out} (°C)	$\dot{W}$ (MW)			
CO_2 comp	∑C_i (up to 75 bar)	50	145–150[b]	−4.70	−0.46	−5.03	−0.16

[a] Several streams at different temperatures can be fed into a heat exchanger (T_1/T_2).
[b] The temperature of this stream may vary within a range (T_1-T_2).
[c] The stream at 850 °C is only fed to ER-CaO under SC2 since it corresponds to the recirculation from SSU to CR.

storage required under this pair of calciner/carbonator loads.

4.4. Heat availability and demand

The amount of available and demanded heat in the equipment under the whole range of situations included in the operation maps defined in Sections 4.2 and 4.3 are now assessed in detail. This information will be useful to understand the range of values in which each heat exchanger will be operated. However, the information presented in this section is aggregated and a more detailed and individual analysis of the behaviour of each independent heat exchanger is beyond the scope of this work.

When EROM is analysed, the threshold operation points which maximize the thermal availability presented in Fig. 5 are assessed. These operation points correspond to the pairs of reactor loads (L_{CL}, L_{CR}): (0.8, 1), (0.4, 0.5), (0, 1) and (0, 0.5). In SC1, the corresponding pairs of storage and discharge fractions ($f_{st,CaCO3}$, $f_{dch,CaCO3}$) are (0.7, 0.5), (0.5, 0.4), (1, 0.1) and (0.5, 0.1) while in SC2, they are (0.5, 0.3), (0.5, 0.4), (1, 0.1) and (0.5, 0.1). The operation map for ESOM is also analysed through the assessment of the limit operation points which maximize the energy storage efficiency as presented in Fig. 8. These threshold operation points correspond to the pairs of reactor loads (L_{CL}, L_{CR}): (0.6, 0.5), (1, 0.9), and (1, 0.5). Under SC1 and SC2, the corresponding pairs of CaO storage and discharge fractions ($f_{st,CaO}$, $f_{dch,CaO}$) are (0.5, 0.4), (0.5, 0.4) and (0.6, 0.2).

4.4.1. Available heat

The available heat at different levels of temperature under EROM threshold operation points is represented in Fig. 10. The size of the heat exchange equipment is reduced to near a half when solids are separated and non-reacted CaO recirculated to the carbonator. It might be observed when the system is operated under EROM, the availability of very high-temperature heat (950–850 °C) is extremely low or it does not exist.

Under ESOM, the available heat for different levels of temperature in the threshold operation points is represented in Fig. 11. The range of operation of the heat exchangers under ESOM is much narrower than

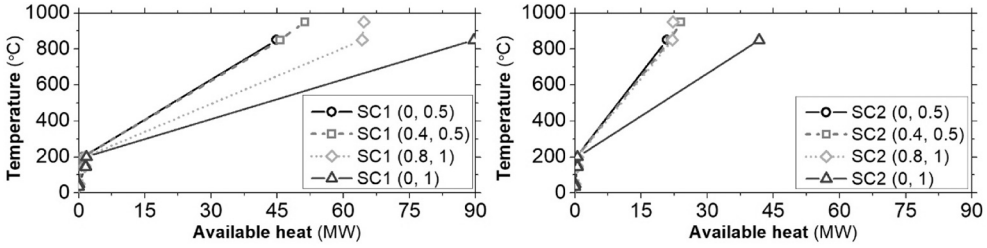

Fig. 10. Available heat at different temperatures for the threshold operation points in EROM (SC1 and SC2).

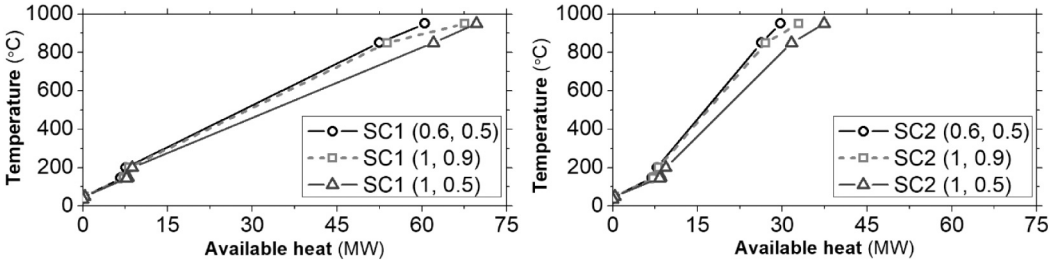

Fig. 11. Available heat at different temperatures for the threshold operation points in ESOM (SC1 and SC2).

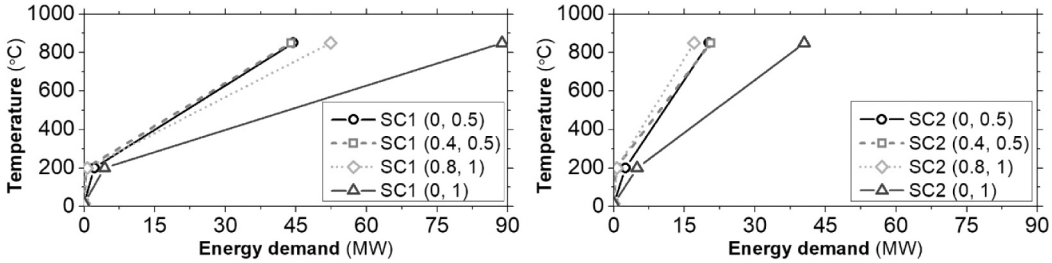

Fig. 12. Energy demand at different temperatures for the threshold operation points in EROM (SC1 and SC2).

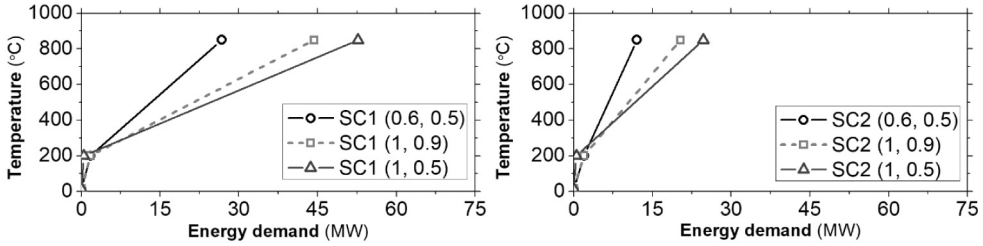

Fig. 13. Energy demand at different temperatures for the threshold operation points in ESOM (SC1 and SC2).

under EROM, facilitating the efficient operation of these equipment. Again, the presence of a solid separation unit (SC2) at the outlet of the carbonator reduces by approximately a half the size of the heat exchangers.

4.4.2. Demanded heat

The demanded heat for different levels of temperature under EROM threshold operation points is represented in Fig. 12. The size of the heat exchange equipment is extremely increased when no separation of solids is implemented. The strong reduction of the demanded heat is a very strong advantage of the inclusion of a solid separation unit. Further research must be done to determine the amount of demanded heat which can be covered with the available heat in the CaL TCES system and the amount which must be provided by external source.

Under ESOM, the demanded heat for different levels of temperature in the threshold operation points is represented in Fig. 13. The demand of thermal energy is reduced to near a half when the system is operated as an energy storage facility. Again, the separation of carbonated solids strongly limits the requirements of heat in the CaL TCES system.

Under each assessed operating point, the difference between the total amount of available and demanded heat has been computed. The sum of available heat is always greater than the total amount of demanded heat within all the limit operating points under EROM and ESOM. When solar energy is not available ($Load_{CL} = 0$), the SC2 presents a higher difference between available and demanded heat than SC1, up to 75 %. The lower the CaO discharged from the ST2 tank, the smaller the size of the heat exchanger named HE-ER-CaO. Thus, the CaO recirculation into the carbonator (SC2) raises the difference in size between release and demand heat exchangers. When the availability of solar energy increases, the difference between availability and demand of thermal energy is greater in SC1 than in SC2. However, since the greater circulation of solids through the reactors within SC1, larger size is required for the heat exchangers.

5. Conclusions

The novelty of this study relies in three main aspects: (i) the identification of the most suitable operation maps under real operating conditions and (ii) the comparison between two scenarios regarding the management of solids at the outlet of the carbonation reactor and (iii) the quantification of heat power demand and availability.

It has been observed that the operation points which are feasible are limited by technical constraints and the operation map of the CaL TCES system banned a large amount of operation situations. The most suitable operating point under each pair of calciner/carbonator loads was selected according to: (i) maximization of thermal energy availability under EROM and (ii) maximization of stored energy efficiency under ESOM. The thermal energy availability for the operation map defined under EROM ranges between 56 and 91 % for both scenarios (SC1 and SC2). Energy storage efficiency is an average 16 % lower for EROM than for ESOM (max energy storage efficiency).

The separation of carbonated solids leads to an increase of the thermal energy availability and an improvement of energy storage efficiency. The specific storage consumption is strongly decreased when solids are completely separated. It can be concluded that the separation of solids improves the performance of the CaL TCES system under both modes of operation.

Regarding plant equipment size, the ER-CaCO3 heat exchanger

power demand can be reduced a 50 % if the criterion of maximum available energy is applied. While if the maximization of energy storage efficiency criterion is applied, the size of the equipment involved in the CaO and CO_2 storage lines (EE-CO2, EE-CaO and compression-cooling train) could be reduced a 40 %, in addition to the 50 % reduction in the ER-CaCO3 heat exchanger size. Comparing the ideal and complete separation of solids scenario (SC2) with the scenario without solid separation (SC1), a size reduction from 53 to 74 % could be reached in the heat exchangers influenced by solid streams (EE-CaO, EE-CaO-P, ER-CaO, EE-CaCO3 and ER-CaCO3) and by unreacted CO_2 leaving the carbonator (EE-CO2-CR). Regarding the rest of the plant equipment (EE-CO2, ER-CO2 and compression-cooling train), results from SC2 show a size increment between 7 and 15 % in comparison to SC1. In conclusion, the threshold values of stored and recovered energy and the size of the plant equipment are defined.

Future research should focus on the estimation of the real potential of partially carbonated solids separation based on density differences. Once the size of the system will be defined, the detailed integration of heat with the power plant should be carried out as well as the economic assessment of the heat exchange network.

Nomenclature

Symbols

f	fraction, –
L	load, –
$\dot{m}$	mass flow rate, kg/s
$\dot{n}$	mole flow rate, kmol/s
$\dot{Q}$	heat flow rate, MW
P	power, MW
R	molar ratio CaO/CO_2, –
T	temperature, °C
$\dot{W}$	electric flow rate, MW
ΔH_R^0	enthalpy of carbonation, kJ/mol
η	efficiency, –

Subscripts and superscripts

amb	ambient
av	availability
CR	carbonator
CL	calciner
dch	discharge
g	gas
in	input or inlet
max	maximum
nom	nominal
out	output or outlet
p	purge or particle
s	solid
st	storage

Acronyms and abbreviations

CaL	Calcium-looping
CSP	Concentrating Solar Power
DOM	Direct Operation Mode
EE	Energy Emitted
ESOM	Energy Storage Operation Mode
ER	energy required
EROM	Energy Release Operation Mode
EV	expansion valve
HE	heat exchanger
SC	scenario
SH	sensible heat
SSC	specific storage consumption
SSU	solids separation unit
ST	storage tank
TCES	thermochemical energy storage
TES	thermal energy storage

CRediT authorship contribution statement

S. Pascual: Conceptualization, Methodology, Software, Visualization, Writing – original draft. **P. Lisbona:** Conceptualization, Methodology, Writing – review & editing, Visualization. **L.M. Romeo:** Conceptualization, Writing – review & editing, Supervision.

Declaration of competing interest

The authors declare the following financial interests/personal relationships which may be considered as potential competing interests: Sara Pascual reports financial support was provided by Ministerio de Ciencia, Innovación y Universidades. Luis M. Romeo reports financial support was provided by Horizon 2020 Framework Programme. Luis M. Romeo reports financial support was provided by Gobierno de Aragón.

Data availability

Data will be made available on request.

Acknowledgment

The FPU Programme of the Spanish Ministry of Science, Innovation and Universities (FPU 2017/03902) provided financial support for S.P. Ph.D. studies. The research was funded by the EU Horizon 2020 research and innovation programme [GA No 727348], SOCRATCES project. The work described in this paper is supported by the Government of Aragon and cofinanced by FEDER 2014–2020 “Construyendo Europa desde Aragón” (Research Group DGA T46_20R).

References

[1] Concentrating solar power projects, National Renewable Energy Laboratory, 2022. https://solarpaces.nrel.gov/projects. (Accessed 1 July 2022).
[2] A. Zervos, R. Adib (Eds.), Renewables 2022. Global Status Report, REN21 Secretariat, 2022 https://www.ren21.net/wp-content/uploads/2019/05/GSR2022_Full_Report.pdf.
[3] S. Kraemer, in: CSP Doesn't Compete With PV – It Competes With Gas, 2017, pp. 1–3, solarpaces.org/csp-competes-with-natural-gas-not-pv/ (accessed July 1, 2022).
[4] T. Islam, N. Huda, A.B. Abdullah, R. Saidur, A comprehensive review of state-of-the-art concentrating solar power (CSP) technologies: current status and research trends, Renew. Sustain. Energy Rev. 91 (2018) 987–1018, https://doi.org/10.1016/j.rser.2018.04.097.
[5] D. Barlev, R. Vidu, P. Stroeve, Innovation in concentrated solar power, Sol. Energy Mater. Sol. Cells 95 (2011) 2703–2725, https://doi.org/10.1016/j.solmat.2011.05.020.
[6] U. Pelay, L. Luo, Y. Fan, D. Stitou, M. Rood, Thermal energy storage systems for concentrated solar power plants, Renew. Sustain. Energy Rev. 79 (2017) 82–100, https://doi.org/10.1016/j.rser.2017.03.139.
[7] S. Kuravi, J. Trahan, D.Y. Goswami, M.M. Rahman, E.K. Stefanakos, Thermal energy storage technologies and systems for concentrating solar power plants, Prog. Energy Combust. Sci. 39 (2013) 285–319, https://doi.org/10.1016/j.pecs.2013.02.001.
[8] A. Kumar, S.K. Shukla, A review on thermal energy storage unit for solar thermal power plant application, Energy Procedia 74 (2015) 462–469, https://doi.org/10.1016/j.egypro.2015.07.728.
[9] S.J. Wagner, E.S. Rubin, Economic implications of thermal energy storage for concentrated solar thermal power, Renew. Energy 61 (2014) 81–95, https://doi.org/10.1016/j.renene.2012.08.013.
[10] K. Vignarooban, X. Xu, A. Arvay, K. Hsu, A.M. Kannan, Heat transfer fluids for concentrating solar power systems – a review, Appl. Energy 146 (2015) 383–396, https://doi.org/10.1016/j.apenergy.2015.01.125.
[11] E. González-Roubaud, D. Pérez-Osorio, C. Prieto, Review of commercial thermal energy storage in concentrated solar power plants: steam vs. Molten salts, Renew. Sust. Energ. Rev. 80 (2017) 133–148, https://doi.org/10.1016/j.rser.2017.05.084.

[12] A. Mohammad, J. Khoshbaf, H. Groningen, C. Orozco, in: Thermal energy storage in CSP technologies: from commercialized to innovative solutions, 2018, pp. 0–26, https://doi.org/10.13140/RG.2.2.22026.57282.
[13] B. Xu, P. Li, C. Chan, Application of phase change materials for thermal energy storage in concentrated solar thermal power plants: a review to recent developments, Appl. Energy 160 (2015) 286–307, https://doi.org/10.1016/j.apenergy.2015.09.016.
[14] A. Palacios, C. Barreneche, M.E. Navarro, Y. Ding, Thermal energy storage technologies for concentrated solar power – a review from a materials perspective, Renew. Energy 156 (2020) 1244–1265, https://doi.org/10.1016/j.renene.2019.10.127.
[15] Innovation Outlook: Thermal Energy Storage, International Renewable Energy Agency (IRENA), Abu Dhabi, 2020 https://www.irena.org/publications/2020/Nov/Innovation-outlook-Thermal-energy-storage.
[16] O. Achkari, A. El Fadar, Latest developments on TES and CSP technologies – energy and environmental issues, applications and research trends, Appl. Therm. Eng. 167 (2020), 114806, https://doi.org/10.1016/j.applthermaleng.2019.114806.
[17] C. Prieto, P. Cooper, A.I. Fernández, L.F. Cabeza, Review of technology: thermochemical energy storage for concentrated solar power plants, Renew. Sustain. Energy Rev. 60 (2016) 909–929, https://doi.org/10.1016/j.rser.2015.12.364.
[18] R. Barker, The reactivity of calcium oxide towards carbon dioxide and its use for energy storage, Appl. Chem. Biotechnol. 24 (1974) 221–227.
[19] P. Lisbona, M. Bailera, T. Hills, M. Sceats, L.I. Díez, L.M. Romeo, Energy consumption minimization for a solar lime calciner operating in a concentrated solar power plant for thermal energy storage, Renew. Energy 156 (2020) 1019–1027, https://doi.org/10.1016/j.renene.2020.04.129.
[20] X. Chen, Z. Zhang, C. Qi, X. Ling, H. Peng, State of the art on the high-temperature thermochemical energy storage systems, Energy Convers. Manag. 177 (2018) 792–815, https://doi.org/10.1016/j.enconman.2018.10.011.
[21] X. Chen, X. Jin, X. Ling, Y. Wang, Exergy analysis of concentrated solar power plants with thermochemical energy storage based on calcium looping, ACS Sustain. Chem. Eng. 8 (2020) 7928–7941, https://doi.org/10.1021/acssuschemeng.0c01586.
[22] C. Ortiz, J. Valverde, R. Chacartegui, L. Perez-Maqueda, Carbonation of limestone derived CaO for thermochemical energy storage: from kinetics to process integration in concentrating solar plants, ACS Sustain. Chem. 6 (2018) 6404–6417.
[23] H. Sun, Y. Li, Z. Bian, X. Yan, Z. Wang, W. Liu, Thermochemical energy storage performances of ca-based natural and waste materials under high pressure during CaO/CaCO3 cycles, Energy Convers. Manag. 197 (2019) 3–12, https://doi.org/10.1016/j.enconman.2019.111885.
[24] V. Moreno, J. Arcenegui-Troya, P.Enrique Sánchez-Jiménez, A. Perejón, R. Chacartegui, J.Manuel Valverde, L.Allan Pérez-Maqueda, Albero: an alternative natural material for solar energy storage by the calcium-looping process, Chem. Eng. J. 440 (2022), https://doi.org/10.1016/j.cej.2022.135707.
[25] F. Di Lauro, C. Tregambi, F. Montagnaro, P. Salatino, R. Chirone, R. Solimene, Improving the performance of calcium looping for solar thermochemical energy storage and CO2 capture, Fuel 298 (2021), https://doi.org/10.1016/j.fuel.2021.120791.
[26] S. Wu, C. Zhou, P. Tremain, E. Doroodchi, B. Moghtaderi, A phase change calcium looping thermochemical energy storage system based on CaCO3/CaO-CaCl2, Energy Convers. Manag. 227 (2021), https://doi.org/10.1016/j.enconman.2020.113503.
[27] M. Bailera, S. Pascual, P. Lisbona, L.M. Romeo, Modelling calcium looping at industrial scale for energy storage in concentrating solar power plants, Energy 225 (2021), 120306, https://doi.org/10.1016/j.energy.2021.120306.
[28] M. Bailera, P. Lisbona, L.M. Romeo, L.I. Díez, Calcium looping as chemical energy storage in concentrated solar power plants: carbonator modelling and configuration assessment, Appl. Therm. Eng. 172 (2020), 115186, https://doi.org/10.1016/j.applthermaleng.2020.115186.
[29] S. Padula, C. Tregambi, R. Solimene, R. Chirone, M. Troiano, P. Salatino, A novel fluidized bed "thermochemical battery" for energy storage in concentrated solar thermal technologies, Energy Convers. Manag. 236 (2021), 113994, https://doi.org/10.1016/j.enconman.2021.113994.
[30] C. Tregambi, M. Troiano, F. Montagnaro, R. Solimene, P. Salatino, Fluidized beds for concentrated solar thermal technologies—a review, Front. Energy Res. 9 (2021) 1–26, https://doi.org/10.3389/fenrg.2021.618421.
[31] C. Ortiz, A. Carro, R. Chacartegui, J.M. Valverde, Low-pressure calcination to enhance the calcium looping process for thermochemical energy storage, J. Clean. Prod. 363 (2022), https://doi.org/10.1016/j.jclepro.2022.132295.
[32] M. Alvarez Rivero, D. Rodrigues, C.I.C. Pinheiro, J.P. Cardoso, L.F. Mendes, Solid–gas reactors driven by concentrated solar energy with potential application to calcium looping: a comparative review, Renew. Sustain. Energy Rev. 158 (2022), 112048, https://doi.org/10.1016/j.rser.2021.112048.
[33] G. Zsembinszki, A. Sole, C. Barreneche, C. Prieto, A.I. Fernández, L.F. Cabeza, Review of reactors with potential use in thermochemical energy storage in concentrated solar power plants, Energies 11 (2018), https://doi.org/10.3390/en11092358.
[34] C. Ortiz, M.C. Romano, J.M. Valverde, M. Binotti, R. Chacartegui, Process integration of calcium-looping thermochemical energy storage system in concentrating solar power plants, Energy 155 (2018) 535–551, https://doi.org/10.1016/j.energy.2018.04.180.
[35] R. Chacartegui, A. Alovisio, C. Ortiz, J.M. Valverde, V. Verda, J.A. Becerra, Thermochemical energy storage of concentrated solar power by integration of the calcium looping process and a CO2 power cycle, Appl. Energy 173 (2016) 589–605, https://doi.org/10.1016/j.apenergy.2016.04.053.
[36] U. Tesio, E. Guelpa, V. Verda, Integration of thermochemical energy storage in concentrated solar power. Part 2: comprehensive optimization of supercritical CO2 power block, Energy Convers. Manag. 6 (2020), 100038, https://doi.org/10.1016/j.ecmx.2020.100038.
[37] E. Karasavvas, K.D. Panopoulos, S. Papadopoulou, S. Voutetakis, Energy and exergy analysis of the integration of concentrated solar power with calcium looping for power production and thermochemical energy storage, Renew. Energy 154 (2020) 743–753, https://doi.org/10.1016/j.renene.2020.03.018.
[38] R. Bravo, C. Ortiz, R. Chacartegui, D. Friedrich, Hybrid solar power plant with thermochemical energy storage: a multi-objective operational optimisation, Energy Convers. Manag. 205 (2020), 112421, https://doi.org/10.1016/j.enconman.2019.112421.
[39] U. Tesio, E. Guelpa, V. Verda, Comparison of sCO2 and He Brayton cycles integration in a calcium-looping for concentrated solar power, Energy 247 (2022), 123467, https://doi.org/10.1016/j.energy.2022.123467.
[40] R. Bravo, C. Ortiz, R. Chacartegui, D. Friedrich, Multi-objective optimisation and guidelines for the design of dispatchable hybrid solar power plants with thermochemical energy storage, Appl. Energy 282 (2021), https://doi.org/10.1016/j.apenergy.2020.116257.
[41] C. Tregambi, P. Bareschino, E. Mancusi, F. Pepe, F. Montagnaro, R. Solimene, P. Salatino, Modelling of a concentrated solar power – photovoltaics hybrid plant for carbon dioxide capture and utilization via calcium looping and methanation, Energy Convers. Manag. 230 (2021), 113792, https://doi.org/10.1016/j.enconman.2020.113792.
[42] C. Ortiz, R. Chacartegui, J.M. Valverde, A. Carro, C. Tejada, J. Valverde, Increasing the solar share in combined cycles through thermochemical energy storage, Energy Convers. Manag. 229 (2021), 113730, https://doi.org/10.1016/j.enconman.2020.113730.
[43] C. Ortiz, C. Tejada, R. Chacartegui, R. Bravo, A. Carro, J.M. Valverde, J. Valverde, Solar combined cycle with high-temperature thermochemical energy storage, Energy Convers. Manag. 241 (2021), 114274, https://doi.org/10.1016/j.enconman.2021.114274.
[44] S. Pascual, P. Lisbona, M. Bailera, L.M. Romeo, Design and operational performance maps of calcium looping thermochemical energy storage for concentrating solar power plants, Energy 220 (2021), 119715, https://doi.org/10.1016/j.energy.2020.119715.
[45] F. Martinez Castilla, G. Guío-Pérez, D.C. Papadokonstantakis, S. Pallarès, D. Johnsson, Techno-economic assessment of calcium looping for thermochemical techno-economic assessment of calcium looping for thermochemical energy storage with CO 2 capture, Energies 14 (2021) 0–17.
[46] C. Ortiz, J.M. Valverde, R. Chacartegui, L.A. Perez-Maqueda, P. Giménez, The calcium-looping (CaCO3/CaO) process for thermochemical energy storage in concentrating solar power plants, Renew. Sustain. Energy Rev. 113 (2019), 109252, https://doi.org/10.1016/j.rser.2019.109252.
[47] V. Manovic, J.P. Charland, J. Blamey, P.S. Fennell, D.Y. Lu, E.J. Anthony, Influence of calcination conditions on carrying capacity of CaO-based sorbent in CO2 looping cycles, Fuel 88 (2009) 1893–1900, https://doi.org/10.1016/j.fuel.2009.04.012.
[48] G.S. Grasa, J.C. Abanades, CO2 capture capacity of CaO in long series of carbonation/calcination cycles, Ind. Eng. Chem. Res. 45 (2006) 8846–8851, https://doi.org/10.1021/ie0606946.
[49] N. Rodriguez, M. Alonso, G. Grasa, J.C. Abanades, Heat requirements in a calciner of CaCO3 integrated in a CO2 capture system using CaO, Chem. Eng. J. 138 (2008) 148–154, https://doi.org/10.1016/j.cej.2007.06.005.
[50] S. Pascual, F. Di Lauro, P. Lisbona, L.M. Romeo, C. Tregambi, F. Montagnaro, R. Solimene, P. Salatino, Improvement of performance of fluidized bed calcium looping for thermochemical solar energy storage: modelling and experiments, in: Proc. 10th Eur. Combust. Meet, 2021, pp. 1430–1435.
[51] F-Chart, Engineering Equation Solver (EES) software. https://www.fchartsoftware.com/ees/, 2022.
[52] M.W. Chase Jr., NIST-JANAF themochemical tables, in: J. Phys. Chem. Ref. Data, Monogr. 9, Fourth Ed., 1998, pp. 1–1951, https://webbook.nist.gov/cgi/cbook.cgi?ID=C1305788&Type=JANAFS&Plot=on.
[53] G.K. Jacobs, D.M. Kerrick, K.M. Krupka, The high-temperature heat capacity of natural calcite (CaCO3), Phys. Chem. Miner. (1981) 55–59, https://doi.org/10.1007/978-3-642-37015-1_18.